FEBS Letters 540 (2003) 26–34

FEBS 27108

Minireview

Coupling of nuclear wavepacket motion and charge separation in bacterial reaction centers

V.A. Shuvalov[a,b,*], A.G. Yakovlev[a]

[a] *Laboratory of Photobiophysics, Belozersky Institute of Chemical and Physical Biology of Moscow State University, Moscow 119992, Russia*
[b] *Institute of Basic Biological Problems, Russian Academy of Sciences, Pushchino, Moscow Region 142290, Russia*

Received 26 February 2003; accepted 3 March 2003

First published online 14 March 2003

Edited by Vladimir Skulachev

Abstract **The mechanism of the charge separation and stabilization of separated charges was studied using the femtosecond absorption spectroscopy. It was found that nuclear wavepacket motions on potential energy surface of the excited state of the primary electron donor P* leads to a coherent formation of the charge separated states $P^+B_A^-$, $P^+H_A^-$ and $P^+H_B^-$ (where B_A, H_B and H_A are the primary and secondary electron acceptors, respectively) in native, pheophytin-modified and mutant reaction centers (RCs) of *Rhodobacter sphaeroides* R-26 and in *Chloroflexus aurantiacus* RCs. The processes were studied by measurements of coherent oscillations in kinetics at 890 and 935 nm (the stimulated emission bands of P*), at 800 nm (the absorption band of B_A) and at 1020 nm (the absorption band of B_A^-) as well as at 760 nm (the absorption band of H_A) and at 750 nm (the absorption band of H_B). It was found that wavepacket motion on the 130–150 cm^{-1} potential surface of P* is accompanied by approaches to the intercrossing region between P* and $P^+B_A^-$ surfaces at 120 and 380 fs delays emitting light at 935 nm (P*) and absorbing light at 1020 nm ($P^+B_A^-$). In the presence of Tyr M210 (*Rb. sphaeroides*) or M195 (*C. aurantiacus*) the stabilization of $P^+B_A^-$ is observed within a few picoseconds in contrast to YM210W. At even earlier delay (~40 fs) the emission at 895 nm and bleaching at 748 nm are observed in *C. aurantiacus* RCs showing the wavepacket approach to the intercrossing between the P* and $P^+H_B^-$ surfaces at that time. The 32 cm^{-1} rotation mode of HOH was found to modulate the electron transfer rate probably due to including of this molecule in polar chain connecting P_B and B_A and participating in the charge separation. The mechanism of the charge separation and stabilization of separated charges is discussed in terms of the role of nuclear motions, of polar groups connecting P and acceptors and of proton of OH group of TyrM210.**

Key words: Photosynthesis; Reaction center; Electron transfer; Wavepacket; Femtosecond spectroscopy

1. Introduction

The reaction center (RC) of purple bacteria consists of three protein subunits (L, M and H), four bacteriochlorophyll molecules, two bacteriopheophytin molecules, two quinone (Q) molecules and one atom of non-heme iron. The complete three-dimensional structure of RC was established [1–4]. The primary act of charge separation in RC occurs between the excited primary electron donor, P*, bacteriochlorophyll dimer, and a monomeric bacteriochlorophyll B_A forming an intermediate state $P^+B_A^-$ within ~3 ps at 293 K (where A denotes the photoactive branch of cofactors) [5–14]. Then an electron is transferred from B_A^- to bacteriopheophytin H_A within ~1 ps and from H_A^- to Q_A within ~200 ps. Each of these processes is accelerated by two to three times when temperature decreases down to 5–10 K. The formation of P* is accompanied by the bleaching of P absorption bands at 870 and 600 nm and by the appearance of a stimulated emission around 920 nm. The stimulated emission disappears when an electron is transferred from P* to B_A and concomitantly the bleaching of the absorption band of B_A^- at 800 nm and the development of the absorption band of B_A^- at 1020 nm take place. The formation of $P^+B_A^-$ is observed with lower amplitude in native RCs due to ultrafast conversion of the $P^+B_A^-$ state to the lower-laying $P^+H_A^-$ state but it is observed distinctly in RCs in which H_A is replaced by plant pheophytin *a* (Pheo) [11–14]. Since $Pheo^-$/Pheo redox potential has a more negative value than that for bacteriopheophytin, the free energy level of P^+Pheo^- becomes higher than that of $P^+B_A^-$ by ~200 cm^{-1} [15]. Consequently, the electron transfer (ET) from B_A^- to Pheo is delayed significantly. Pheo takes part virtually in ET from B_A^- to Q_A [15], which proceeds with a time constant of 1.8 ns instead of 70 ps observed in native RCs at 5 K [12]. The replacement of H_A by Pheo was found to make no changes in ET from P* to B_A [12]. As revealed by recombination fluorescence measurements [16] the free energy level of $P^+B_A^-$ is below that of P^*B_A by 550 cm^{-1}. The $P^+B_A^-$ recombination time is about 1 ns [12] and is longer than a lifetime of P*B (≈300 ps).

According to the current knowledge ET between P* and B_A should occur at the intercrossing of potential energy surfaces for the P^*B_A and $P^+B_A^-$ states. An effective approach to study of ET events at the intercrossing was recently suggested by the measurements of femtosecond (fs) oscillations in the B_A^- product absorption band at 1020 nm (see for example [13,14]) using fs excitation of P to create a wavepacket on the P^*B_A

*Corresponding author. Fax: (7)-96-7790532.
E-mail address: shuvalov@issp.serpukhov.su (V.A. Shuvalov).

Abbreviations: ΔA, light-minus-dark absorbance changes; B_A, H_A and H_B, monomeric bacteriochlorophyll (B) and bacteriopheophytin (H) molecules located in active branch A and in branch B, respectively; ET, electron transfer; FT, Fourier transform; P*, primary electron donor; Pheo, plant pheophytin; Q, quinone; RC, reaction center

0014-5793/03/$22.00
doi:10.1016/S0014-5793(03)00237-0

potential energy surface as described by Vos et al. [17,18]. As a result the excitation by a very short (≤ 30 fs) light pulse of broad spectral width leads to a superposition of wavefunctions of several vibrational levels instead of one definite vibration.

The emission wavelength of the wavepacket is determined by an energy distance from an emitting point on the P* surface to a point on the potential energy surface of the ground state P, both connected by a vertical line [17,18]. The wavepacket spends a maximal time at two points located on opposite sides of the potential energy surface where its potential energy is maximal and kinetic energy is minimal. The wavepacket appears at these points out of phase once during the oscillation period. In contrast, the wavepacket appears near the surface bottom with maximal impulse twice during the repetition period and spends a minimal time at this point. As a consequence, the emission of the wavepacket fluorescence with out-of-phase oscillations occurs near 895 and 935 nm where the formation of distinct emission maximum is observed [13,14,17–19]. The spectrum of fs oscillations at 10 K obtained by Fourier analysis spreads from 10 to 400 cm^{-1} and consists of the frequencies near 15, 30, 69, 92, 122, 153, 191 and 329 cm^{-1} [18]. Similar vibrational modes were found at 27, 73, 110, 147, 175 and 205 cm^{-1} by photochemical hole burning [20] and at 34, 71, 95 and 128 cm^{-1} by resonance Raman [21]. Small differences in frequency values can be due to usage of RCs isolated from different bacteria (*Rhodobacter sphaeroides* and *Rhodopseudomonas viridis*).

As mentioned the wavepacket is formed by superposition of the wavefuctions of several vibrational levels of the excited state due to a broad excitation spectrum of ultrashort pulses (<30 fs) as follows [22]:

$$\Psi(x,t) = (2m+1)^{-0.5} \sum_{-m<j<m} \varphi_{n+j} \exp\{-i\omega(n+j+0.5)t\}$$

where φ_{n+j} is a fundamental function of harmonic oscillator, ω is a mechanical oscillation frequency, and $2m+1$ is the number of waves forming the wavepacket. Interestingly, the wavepacket behaves like a quasi-classical particle [22].

When the wavepacket is created on the potential energy surface of the P^*B_A state, it begins to move on that surface and approaches the intercrossing with the potential energy surface of the $P^+B_A^-$ state. The wavepacket motion along the reaction coordinate is the necessary condition for this [13,14]. The first step of the conversion was theoretically described in [23] by a harmonic bath model with the electronically diabatic (phonon) Hamiltonians for the ground (PB_A, $H_1 = K+\Sigma_i h\omega_i(x_i-\xi_i/(h\omega_i))^2/2+\Sigma_j h\omega_j y_j^2/2+\varepsilon_1$), locally excited ($P^*B_A$, $H_2 = K+\Sigma_i h\omega_i x_i^2/2+\Sigma_j h\omega_j y_j^2/2$) and charge transfer ($P^+B_A^-$, $H_3 = K+\Sigma_i h\omega_i(x_i-\xi_i'/(h\omega_i))^2/2+\Sigma_j h\omega_j(y_j-\eta_j/(h\omega_j))^2/2+\varepsilon_3$) states (here K denotes the kinetic energy; x_i and y_j are the dimensionless coordinates; ε_1 and ε_3 indicate the energy differences of the potential minima for H_1 and H_3 from H_2). The reaction coordinates Q_1 and Q_2 [23] are defined for the photoexcitation and the ET processes, respectively. The angle (θ) between Q_1 ($\equiv\Sigma_i\xi_i x_i$) and Q_2 ($\equiv\Sigma_i\xi_i' x_i+\Sigma_j\eta_j y_j$) determines the amplitude of the fs oscillation of ET rate.

The results we have presented ([13,14,19,24–27] and see [30–32]) show that in RCs the wavepacket are initially formed by fs light pulses on the 130–140 cm^{-1} potential energy surface of P* at the short-wavelength side of the stimulated emission band from P* (895 nm). No $P^+B_A^-$ is observed at this side. However, ET towards B branch pigments is probably revealed from experimental data (see Sections 6 and 7). Subsequent motion of the wavepacket on the 130–140 cm^{-1} surface towards the long-wavelength side of the stimulated emission band (935 nm) leads it to the intercrossing region between P* and $P^+B_A^-$ surfaces at 120 fs delay with the appearance of the B_A^- band at 1020 nm.

2. Nuclear wavepacket motion coupled to the ET from P* to B_A in Pheo-modified R-26 RCs at 293 and 90 K

We start with the results [13,14,24–26] obtained on Pheo-modified *Rb. sphaeroides* R-26 RCs in which the ET from P* to B_A is not perturbed, but further transfer to H_A is blocked (Figs. 1A and 2A,B).

At 293 and 90 K the difference (light-minus-dark) absorption spectra in the range of 900–980 nm (P* stimulated emission) and 980–1060 nm (B_A^- absorption band) were measured at different fs delays after selective excitation of P by 20-fs pulses at 870 nm. At 293 and 90 K the fs kinetics of light-minus-dark absorbance changes (ΔA) at 900, 935 and 1020 nm were derived from the transient ΔA spectra. For this purpose, the amplitudes of ΔA at 900, 935 and 1020 nm were calculated as demonstrated by the arrows in the inset of Fig. 3. The kinetics at 805 nm were measured directly (see [19,27]). At 17 fs the stimulated emission from P* has a maximum near 895 nm. No band near 1020 nm is observed at this delay. A subsequent red shift to $\sim$935 nm of the stimulated emission

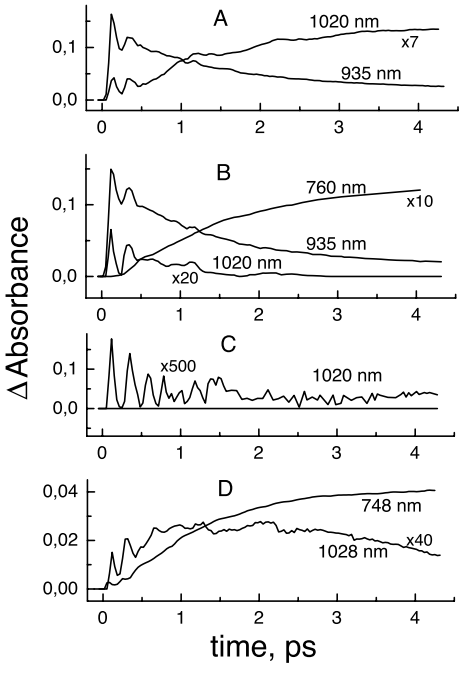

Fig. 1. A: Kinetics of the 935-nm band of P* stimulated emission and of the 1020-nm band of the state $P^+B_A^-$ in Pheo-modified *Rb. sphaeroides* R-26 RCs. B: Kinetics of the 935-nm band, 1020-nm band and 760-nm band of the $P^+H_A^-$ state in native R-26 RCs. C: Kinetics of the 1020-nm band of the $P^+B_A^-$ state in the YM210W mutant of R-26 RCs and its dry film (close to the zero line). D: Kinetics of the 1028-nm band of the $P^+B_A^-$ state and of the 748-nm band of the $P^+H_B^-$ state in *C. aurantiacus* RCs. Measurements were done at 90 K using 20-fs excitation at 870 nm. Data are taken from [26].

band observed at ~120 fs delay is accompanied by an appearance of the band at 1020 nm (Fig. 1A) which disappears again at 250 fs concomitantly with a blue shift of the stimulated emission back to 895 nm, etc. Since the 1020-nm absorption band belongs almost solely to the radical anion band of the bacteriochlorophyll B_A (see [12] for references) these data show that the oscillations in the stimulated emission from P* are accompanied by the oscillations in the reaction product $P^+B_A^-$.

The period of initial intensive oscillations is about 240–260 fs for all kinetics, which corresponds to the oscillation frequency of about 130–140 cm^{-1}. The oscillations in the stimulated emission at 935 nm are out of phase with those at 900 nm [13,14,17,18] The oscillations in the bleaching at 805 nm and in the absorption appearance at 1020 nm, both of which are characteristic of the $P^+B_A^-$ state formation (see [12]), are in phase to each other and to oscillations in the stimulated emission at 935 nm (see Fig. 1 and [13,14,19,27]). These data strongly suggest that when the wavepacket emits fluorescence at 935 nm it locates near the intercrossing between the P^*B_A and $P^+B_A^-$ potential energy surfaces. In contrast, the wavepacket is far away from the intercrossing of two surfaces when it emits fluorescence at 895 nm since the appearance of this fluorescence is not in phase with the $P^+B_A^-$ formation. However the emission at 895 nm is in phase with or close to the $P^+H_B^-$ formation in *Chloroflexus aurantiacus* RCs (see below). The relative amplitudes of the oscillations at 935 and 1020 nm at 120 fs delay measured with respect to maximal amplitudes of corresponding ΔA (found as a difference between 250-fs and 7-ps delays) are approximately the same (0.19 and 0.2, respectively). It suggests that in the intercrossing region the wavepacket emits at 935 nm (P*) and absorbs at 1020 nm (B_A^-). The time of the wavepacket at the intercrossing is about 100 fs at 120 fs delay measured as a halfwidth of the 1020 nm kinetic peak near 120 fs delay (Fig. 1).

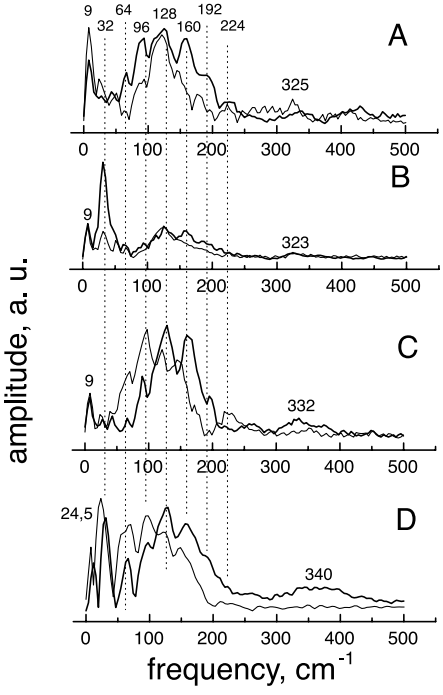

Fig. 2. FT spectra of the oscillatory part of: the 935-nm kinetics for pheophytin-modified RCs of *Rb. sphaeroides* R-26 RCs (thick curve) and its dry film (thin curve) excited by 20-fs pulses at 870 nm and at 90 K (A); the 1020-nm kinetics of Pheo-modified R-26 RCs (thick curve) and its dry film (thin curve) (B); the 935-nm kinetics of native R-26 RCs in HOH buffer (thick curve) and in DOD buffer (thin curve) (C); the 1020-nm kinetics of native R-26 RCs in the HOH buffer (thick curve) and in the DOD buffer (thin curve) (D). Data are taken from [26].

The frequency of 140 cm^{-1} has earlier been registered in the fs measurements of stimulated emission at 10 K [18] and in the hole burning spectra [20]. This mode was found to be a basic one underlying the long-wavelength absorption band of P at various temperatures [28,29]. These observations taken together with the results obtained in the fs measurements make it highly probable that the 130–140 cm^{-1} mode activated upon excitation at 870 nm is coupled to the $P \rightarrow P^*$ optical transition.

After 400 fs delay another type of oscillations with a period of 1 ps (a frequency of ~32 cm^{-1}) is discerned in the kinetics of ΔA at 1020 and 805 nm [13,14,24–27] (90-K measurements are presented in Figs. 1 and 2). These lower-frequency oscillations superimposed on the exponential (~3 ps rise time at 293 K and ~1.5 ps at 90 K [26]) growth of the 1020-nm band and bleaching of the 800-nm band [19,27] can be more clearly seen after subtracting the exponential part of ΔA.

The starting time at ~100 fs for the 32 cm^{-1} mode oscillation can be estimated by an extrapolation of the oscillations to zero fs delay. This starting time allows to suggest that the 32 cm^{-1} mode is activated at the moment when the wavepacket moving on the 130–140 cm^{-1} potential energy surface approaches the intersection with $P^+B_A^-$ surface for first time at 120 fs. The time of the wavepacket at the intersection is about 600 fs at 1 ps delay.

The results of the Fourier transform (FT) of the oscillatory part of the 935- and 1020-nm-band kinetics at 293 K are similar to those at 90 K and will be discussed below.

3. Nuclear wavepacket motions coupled to ET in native RCs at 293 and 90 K

Now we show the results obtained for native *Rb. sphaeroides* R-26 RCs in which the ET from B_A to H_A occurs.

Oscillations measured for Pheo-modified RCs (see above) in the fs kinetics of the 1020-nm absorption band development are also observed for native RCs of *Rb. sphaeroides* R-26 at 293 K [25] and 90 K ([26] and Fig. 1B). Again, the amplitudes of ΔA for kinetic measurements were revealed from difference absorption spectra measured at different delays (amplitude measurements are demonstrated by arrows in the inset of Fig. 3). The spectra and kinetics show that the B_A^- band at 1020 nm firstly appears at a delay of ~120 fs with the amplitude comparable to that observed in Pheo-modified RCs and almost completely disappears at 250 fs. This reversible development of the 1020-nm absorption band is in phase with the first appearance of the stimulated emission band at 935 nm, in agreement with measurements performed on the Pheo-modified RCs (see [13,14,25,26] and Fig. 1A). The second appearance of the 1020-nm band is observed at ~380 fs (~260-fs period of oscillation corresponding to a frequency of ~130 cm^{-1}), which is in phase with the stimulated emission at 935 nm and is ~70% reversible. Next three oscillations of the 1020-nm band at 293 K are observed at ~1.15 ps (~50% reversibility), ~2.17 ps and 3.14 ps with a halfwidth of about 680 fs (~1-ps period corresponding to a frequency

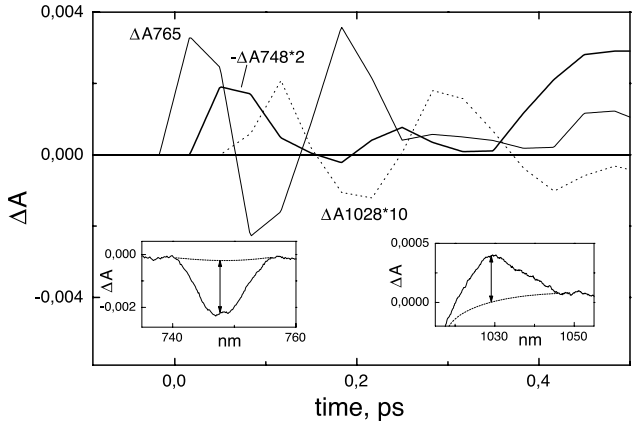

Fig. 3. Kinetics of ΔA within first 500 fs at 765, 748 and 1028 nm for *C. aurantiacus* RCs excited by 20-fs pulses at 870 nm and at 90 K. Insets show the difference absorbance spectra measured at 117 fs delay for 1028 nm and at 51 fs delay for 748 nm after subtraction of the spectrum measured at 17 fs delay (see text for details).

of $\sim$33 cm^{-1}). In contrast to Pheo-modified RCs (Fig. 1) the non-oscillating amplitude of the 1020-nm band at 293 K was estimated to increase within $\sim$0.9 ps and decrease within $\sim$2.5 ps due to the ET from P* to B_A ($\sim$2.5 ps) and from B_A^- to H_A ($\sim$0.9 ps) in native RCs, in agreement with earlier estimations [10]. At 90 K the rise time is about $\sim$300 fs and the decay time is about 1.5 ps (Fig. 1B) due to the acceleration of both processes.

The results of the FT of the oscillatory part of the 935- and 1020-nm-band kinetics at 293 K are similar to those at 90 K and will be discussed below.

The kinetics of the bleaching of Q_Y absorption band of the photochemical active bacteriopheophytin (H_A) at 760 nm due to the formation of the state $P^+H_A^-$ in native RCs of *Rb. sphaeroides* R-26 were measured at 293 K [25] and 90 K ([26] and Fig. 1B). Amplitude of the 760-nm-band bleaching (ΔA_{760}) was calculated on the basis of the difference absorption spectra. From a comparison of the kinetics of absorbance changes in the 1020-nm band and in the 760-nm band at 293 K it was found that the ET from B_A^- to H_A starts when the 32 cm^{-1} mode peaks are observed at $\sim$1.15, $\sim$2.17and $\sim$3.14 ps. No ET to H_A is observed when B_A^- appears at the intercrossing of the P* and $P^+B_A^-$ surfaces at 120 and 380 fs delays at 293 K [25]. An analysis of the kinetics of the 1020- and 760-nm bands has shown that an increase in the bleaching of the 760-nm band represents roughly integration over the time of the 1020-nm oscillatory peaks at $\sim$1.15, $\sim$2.17 and $\sim$3.14 ps superimposed on smooth growth [25]. It means that the motion of the wavepacket on the $P^+B_A^-$ surface is accompanied by a proportional ET to H_A. The study of the kinetics at 760 nm at 90 K ([26] and Fig. 1B) shows that such integration occurs at a much earlier time when the 1020-nm peak appears at 380 fs. In agreement with that the kinetics at 1020 nm are very much different at 293 and 90 K. At 293 K fs oscillations are superimposed on the quasi-exponential rise ($\sim$1 ps) and decay ($\sim$3 ps) of the absorbance changes. At 90 K, after the peaks at 120 and 380 fs, the 1020-nm band decays rapidly to zero ([26] and Fig. 1B).

The FT of the oscillatory part of the 760-nm-band kinetics has shown that the spectrum includes the dominant band at 32 cm^{-1} [25], in agreement with the measurements at 788 nm at low temperature [33]. Since this frequency is similar to that observed for the 1020-nm-band kinetics this fact supports the idea that the 32 cm^{-1} mode includes the intersurface motion of the wavepacket between the P* and $P^+B_A^-$ surfaces accompanied by the ET to H_A.

4. The coupling between nuclear wavepacket motion and ET studied in more details at 90 K

At 90 K all kinetics at 935 and 1020 nm (or 1028 nm; Fig. 1) and FT spectra of oscillatory parts presented in [26] and Fig. 2 include oscillations with a fundamental frequency of 32 cm^{-1} and its overtones around 64 (second harmonics, 2), 96 (3), 128 (4), 160 (5), 192 (6) and 224 (7) cm^{-1}. The amplitude of the 32 cm^{-1} peak in the FT spectrum of the dry film of Pheo-modified RCs is decreased by a factor of $\sim$4.7 (Fig. 2B). The overtones of this mode observed in the solution are decreased by the same factor in the 935-nm oscillations (Fig. 2A). Only the vibrational mode around 122 cm^{-1} is observed. It means that the $\sim$125 cm^{-1} mode seems to induce the 32 cm^{-1} mode overtones in hydrated preparations. All studied kinetics have a different ratio between amplitudes of the fundamental oscillation at 32 cm^{-1} and its overtones. For each electronic state this ratio can be explained in terms of efficiency and reversibility of further ET: the more effective ET and the less reversibility the smaller the amplitude of the corresponding peak in the FT spectrum. An opposite situation takes place for the product: the more effective ET and the less reversibility the larger the amplitude of the peak in the FT spectrum of the product. From Fig. 2 one can conclude that the most effective nuclear motion for total ET from P* to H_A has a frequency at 32 cm^{-1} [13,14,24–26,33]. The same 32 cm^{-1} frequency is effective for the stabilization of the first charge separated state $P^+B_A^-$. Therefore this mode is suppressed in the kinetics of the P* decay in both native and Pheo-modified RCs. For the same reason the 32 cm^{-1} mode is enhanced in the $P^+B_A^-$ kinetics in Pheo-modified RCs but not so much in native RCs, in which further ET to H_A takes place. Finally this mode is the main one in the $P^+H_A^-$ kinetics in native RCs [25,26]. In contrast, the higher overtones are not accompanied by an effective stabilization of the $P^+B_A^-$ state. As a result, the enhanced overtones (3–6) are observed in the P* decay kinetics (Fig. 2). Their amplitudes are smaller in the kinetics of the $P^+B_A^-$ formation, and almost no harmonics higher than three are present in the kinetics of the formation of $P^+H_A^-$ [25,26].

The 1020-nm-band peaks seen in Pheo-modified RCs at 1.14, 2.17 and 3.2 ps are characterized by a sine-like shape (Fig. 1A). These peaks are separated by an interval of $\sim$1.03 ps (32 cm^{-1}). Extrapolation of this series back to zero delay gives a value of $\sim$100 fs, which corresponds to the first oscillation peak in the P* stimulated emission at 935 nm and in the B_A^- development at 1020 nm. However, at 120 fs delay there is a 1020-nm peak with a much narrower width ($\sim$100 fs) corresponding to that for the 935-nm emission from P* (125 cm^{-1} mode; Fig. 1). The mode at 125 cm^{-1} is clearly seen in the dry film of RCs when the 32 cm^{-1} mode and its overtones are suppressed (Fig. 2A). We suggest therefore that the appearance of the wavepacket in the intercrossing area between the P* and $P^+B_A^-$ potential energy surfaces at 120 fs leads to the transformation of the 125 cm^{-1} mode (probably vibrational) into the 32 cm^{-1} mode and its overtones on the P* hypersurface. The higher overtones are populated in

the 935-nm kinetics according to the energy difference between the 125 cm^{-1} vibrational mode and specific overtones of the 32 cm^{-1} mode (Fig. 2A).

The 32 cm^{-1} mode and its overtones are of interest for further discussion. The presence of higher harmonics is not characteristic of vibrational modes. The appearance of several harmonics in P* stimulated emission oscillations (Fig. 2) might indicate that these oscillations are related to a rotation of small molecules like OH^- or H_2O, located between the photochemical active RC chromophores. This assignment is tentative and does not exclude other possibilities. Another important point is related to the relative amplitude of oscillations (~35%, see Fig. 1). It means that all suggestions deal with this limited percentage of RCs.

In X-ray model of *Rp. viridis* RCs only two HOH molecules are known to be present between P and B_A and between P and B_B (see Brookhaven Protein Databank, 1PRC). Based on the angle (~104°) and distances between corresponding atoms (~3 Å) it is reasonable to suggest that the water molecule, HOH302, can have hydrogen bond to the N atom of HisM200 (which serves as the axial ligand to the magnesium of P_B) on the one side and to the keto carbonyl group of ring V of B_A on the other side (Fig. 4). The possible weakness or absence of the hydrogen bond between HOH and B_A observed by resonance Raman (see [21,34,35]) would be consistent with a rotation of HOH with parameters close to the gas phase. An alternative explanation might be that HOH rotation can occur after RC excitation when all hydrogen bonds of HOH (if they are existing) are broken. The rotational spectra of small molecules in the gas phase include many lines reflecting a population of many harmonics [36].

Three types of rotation of two protons around oxygen are possible for H_2O. The values of ν for H_2O equal to ~32, ~52, and ~20 cm^{-1} can be found [26]. The 32 cm^{-1} mode and the frequency difference between two other modes (32 cm^{-1}) are equal to the 32 cm^{-1} mode observed in RCs. It is interesting that the 51–52 cm^{-1} mode was observed in RCs in which Q_A was doubly reduced [19] and in the dry film of RCs ([26] and Fig. 2).

These estimates suggest that the peaks at 32, 66, 93, 125, 158, 188, 222 cm^{-1} observed in the FT spectra of oscillations in the 935- and 1020-nm kinetics in Pheo-modified RCs (Fig. 2) are due to the modulation of fs kinetics by the rotation of H_2O molecule. The same is probably true at room temperature [25]. One can further suggest that the modulation is along the reaction coordinate of the primary charge separation reaction $P^* \rightarrow P^+B_A^-$ since all rotational frequencies are observed in the oscillations of the kinetics of the B_A^- band development at 1020 nm.

These suggestions are consistent with the effect of isotopic exchange of HOH by DOD (or DOH) on the FT spectra (Fig. 2C,D). The frequencies at 66, 93, 125, 164 and 194 cm^{-1} seem to belong to the higher harmonics of the 32 cm^{-1} mode, since all these frequencies are shifted by the same factor of ~1.3 after H/D exchange. This finding also indicates that all these frequencies are related to the vibration or rotation of the H containing groups. If the 125 cm^{-1} vibrational mode induces the 32 cm^{-1} mode overtones after light absorption the question about isotopic shift of the 125 cm^{-1} mode arises. According to Fig. 2A the frequency at 122 cm^{-1} seen in a dry film is positioned just in the middle of the 32 cm^{-1} mode overtones after H/D exchange. Thus, the isotopic shift of the 125 cm^{-1} mode seems to be small. Recent direct measurements have shown (Yakovlev A.G., Shuvalov V.A., unpublished results) that this shift is of a factor less than 1.1. One can find that the magnitude of the isotopic shift for the rotation induced by

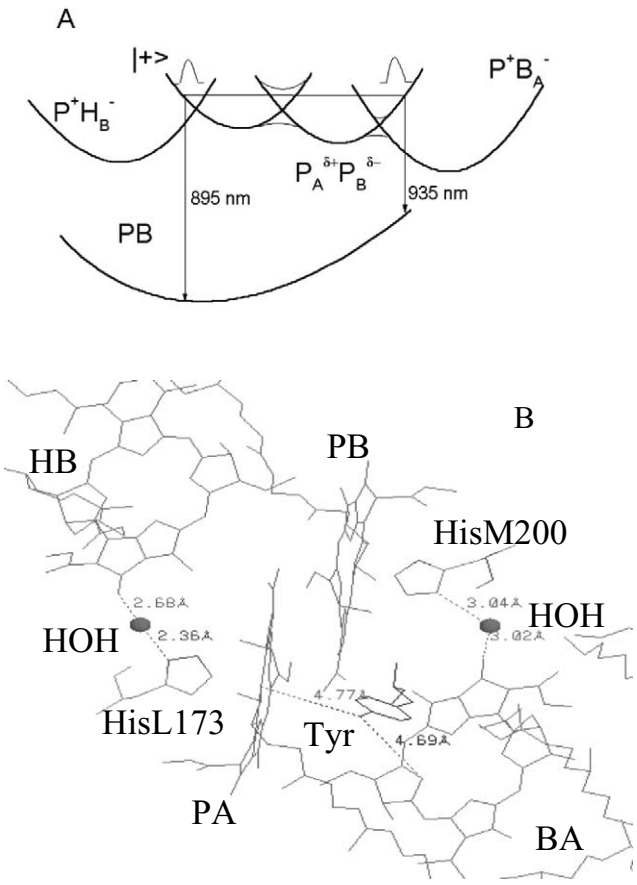

Fig. 4. A: Simplified schematic representation of the diabatic (phonon) potential energy surfaces of the ground ($H_BPB_AH_A$), locally excited ($H_BP^*B_AH_A$) and charge transfer ($H_B^-P^+B_AH_A$, $H_BP^+B_A^-H_A$ and $P^+B_AH_A^-$) states. Strong electronic coupling between P_A and P_B can produce two electronic states in P*: $|+> = \sqrt{1/2}\{|P_A^*P_B> + |P_AP_B^*>\}$ and $|P_A^{\delta+}P_B^{\delta-}>$ with the potential surfaces shifted to each other and split by a large energy coupling. The emission from the surface point with the $|+>$ character is suggested to be near 895 nm and from the point with $P_A^{\delta+}P_B^{\delta-}$ character is near 935 nm due to the larger surface displacement with respect to the ground state. An electronic coupling between P* and B_A (~30 cm^{-1} [59]) splits the two original surfaces (P* and $P^+B_A^-H_A$) into upper and lower surfaces. The surface with the $P_A^{\delta+}P_B^{\delta-}$ character seems to have an intercrossing with that of $P^+B_A^-$ close to the bottom of $P_A^{\delta+}P_B^{\delta-}$. The surface with the $|+>$ character can produce ET to H_B in *C. aurantiacus* RCs. The high-energy (~150 cm^{-1}) wavepacket can approach the upper part of the $P^*B_AH_A$ and $P^+B_A^-H_A$ surface intercrossing and produce emission at 935 nm (P*) and absorption at 1020 nm (B_A^-) with a subsequent reflection back to the P* surface or transmission to the $P^+B_A^-$ surface. B: View (Brookhaven Protein Databank, number 1PRC) of the special pairs of bacteriochlorophylls P_A and P_B, monomeric bacteriochlorophyll B_A and H_B located at the position B_B of *Rp. viridis* RCs. HisM200 liganding Mg of P_B is connected by a hydrogen bond via H_2O to the oxygen of the keto carbonyl group of ring V of B_A. Thus P_B is connected to B_A via a sequence of following polar groups: Mg(P_B)–N–C–N(HisM200)–H–O–H(water)–O=B_A, which can represent a pathway for the ET from P* to B_A. A similar pathway is revealed on the other side of P connecting P_A and B_B (H_B in *C. aurantiacus* RCs). The rotation of the water molecule in such a system with 32 cm^{-1} frequency is induced by the electron flow from P* to B_A (see text for details).

DOD/HOH exchange should be close to 1.9, which is larger than the factor 1.3 found in our experiments. The simplest explanation of this discrepancy is a suggestion about an isotopic fractionation that does not allow complete replacement of both protons by deuterium in water molecules in RCs protein. In other words, the water molecule could be replaced by DOH instead of DOD. This effect is known for other isotopic exchange experiments (see [37] for references). Since measurements at 90 K were done in the DOD buffer with glycerol (65%) containing OH groups, the probability for HOH/DOH exchange may be higher than for HOH/DOD. In this case a factor of 1.4 can be found from calculations, which is close to the factor found experimentally. We do not exclude, however, that the discrepancy between the expected and observed effects points to a possibility of alternative interpretation of the results obtained.

Fig. 4 demonstrates that in the RC of *Rp. viridis* [1,2,38,39] (the structure of which is very similar to that of the *Rb. sphaeroides* RC [4]) 'a bridge' is seen connecting P_B and B_A with the following elements (Brookhaven Protein Databank, number 1PRC): (a) a coordination bond connecting Mg of P_B and N of HisM200 (1.88 Å); (b) a hydrogen bond connecting another N of HisM200 and the oxygen of HOH302; (c) a hydrogen bond connecting the oxygen of HOH302 and the oxygen of the keto carbonyl group of ring V of B_A. Numbers indicate distances. Using experimental data it is tempting to suggest that this bridge including the water molecule can be one of the possible pathways for ET from P* to B_A.

5. The nuclear wavepacket motion and fs ET in natural (YM210L) and gene-engineering (YM210W) mutants of *C. aurantiacus* and *Rb. sphaeroides*, respectively

Fs oscillations in the kinetics at 935 and 1020 nm are observed in the mutant YM210W at 90 K and demonstrate a most simple pattern seen earlier (Fig. 1C). The decay of the stimulated emission at 935 nm and accumulation of the state $P^+B_A^-$ are considerably delayed, especially at low temperature (up to ~300 ps at 90 K), in agreement with earlier observations [41–46]. Even in this case seven peaks of fs oscillations with low amplitude are observed in both kinetics with a period of ~215 fs and a frequency of ~145 cm^{-1} (Fig. 1C). With a relatively smaller amplitude (with respect to native RCs) the higher overtones of the 32 cm^{-1} rotational mode are discerned at 90 K in the FT spectra of the 935-nm kinetics. These overtones disappear in the 935-nm kinetics in the dry film of the mutant YM210W, with a complete disappearance of ET from P* to B_A monitored by the formation of the 1020-nm band of B_A^- (Fig. 1C). This behavior is different from that of Pheo-modified RCs [26] due possibly to a change of the B_A position in the mutant [47]. These facts can be interpreted as an evidence for the involvement of the water molecule in the ET pathway between P* and B_A as suggested earlier [26]. As assumed above the ET from P* to B_A occurs as a result of the ET via a bridge with polar groups between P and B_A: N–Mg(P_B)–N–C–N(HisM200)–HOH–0 = (B_A) (see Brookhaven Protein Databank, 1PRC). In the absence of the ET from P* to B_A and of the rotational mode at 32 cm^{-1} with its overtones in the dry film of the YM210W mutant the vibrational mode at 144 cm^{-1} is clearly revealed with 2d and 3d overtones at 289 cm^{-1} and 434 cm^{-1}, respectively, in the 935-nm kinetics. This demonstrates that the 144 cm^{-1} vibrational oscillations originate inside of the dimer P. They are independent of the presence of the water molecule and of TyrM210. An important observation is revealed that the 144 cm^{-1} vibrational oscillations and the excited state P* itself do not include the 1020-nm-band formation.

In native, Pheo-modified or mutant YM210W R-26 RCs the 130–145 cm^{-1} vibrational oscillations seem to induce the overtones (close in energy to ~140 cm^{-1}) of the water molecule rotational mode at 32 cm^{-1} seen in the 935-nm kinetics of hydrated materials (Fig. 2). The fundamental frequency at 32 cm^{-1} itself (period of ~1 ps) is only observed when the quasi-exponential stabilization of $P^+B_A^-$ occurs within 1.5 ps in Pheo-modified RCs and native RCs at 90 K (Fig. 1 and [26]) or within 3 ps in native and Pheo-modified RCs at 293 K [25] but not in mutant YM210W. This probably means that during the stabilization process the quasi-exponential electron flow from P* to B_A within 1–3 ps induces a relatively slow water molecule rotation at 32 cm^{-1} which modulates ET occurring via the mentioned bridge.

The dynamic stabilization of $P^+B_A^-$ is of interest for further discussion. Two possibilities can be considered. (i) An electron from P* to B_A is transferred to the higher vibrational level on the $P^+B_A^-$ surface with consequent vibrational relaxation to the lowest level according to the well-known model (see [48] for references). (ii) Stabilization takes place due to the reorientation of surrounding groups when $P^+B_A^-$ is reversibly formed. In the latter case the symmetrical arrangement of two surfaces P* and $P^+B_A^-$ can be realized with the maximal possible rate of ET from P* to B_A. When the nuclear motion on the P* surface approaches the intercrossing point between two surfaces both states P* and $P^+B_A^-$ are registered. The wavepacket goes back to the P* surface if there is no additional changes in the nuclear position. However these changes can be induced by reorientation of the surrounding polar group like $O^{\delta-}H^{\delta+}$ of TyrM210 (Fig. 4). In the absence of YM210 the oscillations with a period of 215 fs at 1020 nm are not perturbed within ~1.5 ps (Fig. 1C). It would mean that the motion of $H^{\delta+}$ of OH-TyrM210 toward B_A^- can lower the energy of $P^+B_A^-$ with respect to that of P* stopping coherent oscillations in the system.

The estimations of the energy difference in the system were done for two positions of $H^{\delta+}$ of OH-TyrM210 with respect to P_A and B_A having mostly positive and negative charges, respectively, in $P^+B_A^-$ [40]. In the first position, a dipole $O^{\delta-}H^{\delta+}$ of TyrM210 is perpendicular to a line running between C–N(IV) of P_A and N(II) of B_A which are closest neighbors to TyrM210 and mostly populated by positive and negative charges, respectively, in the state $P^+B_A^-$ [40]. This position was suggested to correspond to the neutral states PB_A or P^*B_A. In the second position, $H^{\delta+}$ of OH-TyrM210 is on a line connecting $O^{\delta-}$ of OH-TyrM210 and N(II) of B_A. This position is assumed to be realized when $H^{\delta+}$ is attracted and repulsed by B_A^- and P_A^+, respectively, in the stabilized state $P^+B_A^-$. The energy difference between the two positions was estimated to be ~890 cm^{-1}. Experimental energy difference between P* and $P^+B_A^-$ in the stabilized state $P^+B_A^-$ for Pheo-modified RCs was found to be 350–550 cm^{-1} [16,49].

Estimation of the time for a shift (s) of $H^{\delta+}$ from the first toward the second position due to the Coulomb attraction and repulsion of $H^{\delta+}$ by the charged atoms of B_A^- and P_A^+, respectively, separated by distances r_{ij} during ~100 fs of each

oscillation, was done by means of the following expression for the distance (s) covered by $H^{\delta+}$ during the time (t) of oscillation: $s = t^2/2\Sigma_{i,j}e^2\gamma_{i,j}/(\varepsilon r_{ij}^2 m)$, where e is an elementary charge, $\gamma_{i,j}$ is a coefficient for electron density on atoms, ε is a dielectric constant of the media, m is a mass of H. The estimation shows that in 65% of RCs an electron is stabilized on B_A (due to the shift of $H^{\delta+}$ from the first to second position) at the 5th peak of fs oscillations at ~1 ps (τ_e) at 0 K. This is consistent with earlier data [50] and Fig. 1. This estimation seems to support the suggestion that the stabilization of $P^+B_A^-$ is provided by a reorientation of $H^{\delta+}$ of OH-TyrM210 with ET from P* to B_A.

C. aurantiacus RCs contains leucine at the analogous position M208, thus representing 'a natural mutant YM208L'. RCs of *C. aurantiacus* demonstrate another example of ET [51–57]. Initial charge separation is delayed down to 7 ps at 296 K. At 10 K two components for P* decay were observed with time constants of 2 and 24 ps. It was suggested that ET might be possible in B branch as well.

For *C. aurantiacus* RCs at 90 K Fig. 1 shows fs oscillations corresponding to FT spectra including the vibrational mode around 160 cm^{-1} and water molecule rotation modes at 35 and 52 cm^{-1} with their overtones (not shown). The amplitude of the fs oscillations at 1028 nm is smaller than that for native *Rb. sphaeroides* R-26 RCs at 1020 nm by a factor of ~10 and similar to that for the mutant YM210W. The reason for this seems to be related to the absence of Tyr at the M210 (M208 in *C. aurantiacus*) site. If the $H^{\delta+}$ of OH-TyrM210 is shifted toward B_A in the dark it can lower the energy of $P^+B_A^-$ with respect to P* in native R-26 RCs up to 890 cm^{-1}. In the absence of TyrM210 the energy of $P^+B_A^-$ may be above that of P* as suggested earlier [42,43]. Then the intercrossing point of the P* and $P^+B_A^-$ surfaces might be above the wavepacket energy. This can be a case for the mutant YM210W of R-26 RCs but not for *C. aurantiacus* RCs since the redox potential of P/P^+ is lower by 70–90 mV than that for R-26 [51,52]. Therefore the reason for the small amplitude of fs oscillations in *C. aurantiacus* RCs seems to be different and is discussed below. The stabilization of $P^+B_A^-$ occurs in *C. aurantiacus* RCs probably due to the presence of another TyrM195 located close to P. The stabilization takes a longer time of ~6 ps at 90 K than in R-26 RCs (1.5 ps). This can be related to a non-symmetrical position of TyrM195 with respect to P_A and B_A (in contrast to that for TyrM210, see Fig. 4) and to a relatively low amplitude of fs oscillations for the $P^+B_A^-$ formation in *C. aurantiacus* RCs.

The tyrosine at the position M210 (or M208) seems to be responsible for the high fs oscillation amplitude in native R-26 RCs due to lowering of the energy level of $P^+B_A^-$ with respect to P* in the dark. Fig. 4 and the atomic coordinates of 1PRC (Brookhaven Protein Databank) show that the angle between atoms C–O–(TyrM210) and both N–(HisM200) and O–(HOH302) and O–(keto group of ring V of B_A) and N(II)–(B_A) lies in the range of 90–100°. This means that the $H^{\delta+}$ of TyrM210 might follow the ET from P* to B_A via the polar group bridge mentioned above. If the $H^{\delta+}$ of TyrM210 is directed to both N^- of HisM200 or to O^- of HOH302 it lowers the Coulomb interaction energy by ~350 cm^{-1} when the reversible fs ET between P* and B_A occurs via these groups. In the second position the $H^{\delta+}$ of TyrM210 is directed to N(II) of B_A with lowering of the energy by ~890 cm^{-1}. In the absence of TyrM210 (or M208) the energy levels of all intermediate states are increased but less for the first position (350 cm^{-1}) and much more for the second position (890 cm^{-1}) of $H^{\delta+}$ and for an electron transferred via the polar bridge. Even for *C. aurantiacus* the increase of the energy level of P* does not completely improve the situation for ET since an electron has some energy barriers (~550 cm^{-1}) for ET from P* to B_A. This might be a reason for the low amplitude of the fs oscillations in native and gene-engineering mutants.

6. Nuclear wavepacket governs the ET in A and B branches of pigments in *C. aurantiacus* at 90 K

The excitation of P in the *C. aurantiacus* RCs at 90 K by 20-fs pulses at 870 nm leads simultaneously to a red shift of the 760-nm band of Bpheo in phase with the 900-nm stimulated emission and out of phase with the 945-nm emission from P* (not shown). The development at 765 nm and the bleaching at 750 nm with a smaller amplitude with respect to the development characterize this shift at 17 fs delay. The sensitivity of the Bpheo-band shift to the P* formation might indicate the appearance of the charge close to H_B when P is excited by 20-fs pulses. If the shift at 17 fs was subtracted from the spectra measured at latter delays the pure bleaching at 748 nm is observed as shown in the inset of Fig. 3. This bleaching is obviously due to the band bleaching of Bpheo (probably H_B) located in the B branch closest to P. Fig. 3 shows the initial fs kinetics for the development at 765 nm due to P* formation, 'pure' bleaching at 748 nm due to H_B^- formation and development at 1028 nm due to the B_A^- formation. The first 1028-nm peak appears ~90 fs later than the first 765 nm peak. Both kinetics are out of phase with each other. The first peak of the 748-nm bleaching appears ~40 fs later than the first 765-nm peak. These observations can be preliminarily interpreted as an indication of the ET to B branch Bpheo molecule when a wavepacket is firstly formed on the P* surface before the formation of the 935-nm stimulated emission and ET form P* to B_A. Latter accumulation of the state $P^+B_A^-$ is accompanied by the accumulation of the state $P^+H_A^-$ as normally occurs in native *Rb. sphaeroides* RCs (Fig. 1).

7. The potential energy scheme for non-equilibrium conversion of the excited state P* into the charge separated states

The described results allow to draw the potential energy scheme for non-equilibrium conversion of the excited state P* into the charge separated states ($P^+H_B^-$, $P^+B_A^-H_A$, $P^+B_AH_A^-$) in bacterial RCs. The first step of the conversion was theoretically described in [23] as mentioned above. The remarkable oscillations in the product at 1020 nm in R-26 RCs as well as at 1028 nm ($P^+B_A^-$) and 748 nm ($P^+H_B^-$) in *C. aurantiacus* RCs indicate that the angle θ is not far away from 180° (and $\cos\theta \approx -1$) in these cases (see Section 1). Therefore one can cut the diabatic potential energy surfaces along the Q_1 and Q_2 coordinates. The results of one-dimensional cross-section are shown in Fig. 4A.

Since the bacteriochlorophyll dimer P has an asymmetrical electron density distribution in the state P^+ in which the electron π-spin density is mostly located on the P_A half of the dimer (0.74/0.26) [40], the upper orbital of the ground state of P should be mostly formed by the orbitals of P_A. The 20-fs excitation of P leads to the formation of a wavepacket on

the surface of the lower excitonic state $\sqrt{1/2}\{|P_A{*}P_B> + |P_AP_B{*}>\} \equiv |+>$ with emission at 895 nm. According to quantum mechanical calculations [58] the hopping time of the local exciton between $P_A{*}$ and P_B is proportional to $\pi h/\Delta E$ where ΔE is an exciton energy splitting in the dimer of ~ 1000 cm^{-1}. This corresponds to $t_{1/2} = 17$ fs. Therefore the 20-fs excitation of P might lead mostly to the formation of a wavepacket with a character of $P_A{*}P_B$. The formation of $P_A^{\delta-}P_B^{\delta+}$ is probably forbidden at this delay since the energy level of LUMO of P_A is higher than that of P_B. The formation of $P_A^{\delta+}P_B^{\delta-}$ is possible but reorganization energy seems to be too high at this point on the potential surface. ET from $P_A{*}$ to B_B is forbidden since the energy level of LUMO of B_B is higher than that of P_A according to calculations [40]. However ET from $P_A{*}$ to H_B in *C. aurantiacus* is possible since the energy of LUMO of H_B is certainly lower than that of $P_A{*}$ and nuclear configuration at the 895-nm emitting side seems to be optimal for it. This is probably realized and revealed by fs 748-nm bleaching (Fig. 3).

The $P_A^{\delta+}P_B^{\delta-}$ surface can probably be approached by the nuclear wavepacket motion on the $\sim$140–160 cm^{-1} surface of $|+>$ at latter delay of $\sim$120 fs when P* emits light at 935 nm and the formation of the 1020-nm (1028 nm in *C. aurantiacus*) band of B_A^- is observed (Fig. 1). In this case a much greater fraction of $P_A^{\delta+}P_B^{\delta-}$ seems to be formed and accelerates ET to B_A. However the possibility that $P_B{*}$ induces ET to B_A directly is not excluded. The necessity of the nuclear motion to the 935-nm emitting side to get ET from P* to B_A supports the first suggestion. The formation of $P_A^{\delta+}P_B^{\delta-}$ can be efficient since the electron π-spin density in P* is mostly located on the P_B half (0.74/0.26) of the dimer, in agreement with calculations [40].

As mentioned above we assume that ET from P* to B_A occurs via polar groups bridge as follows: N–Mg(P_B)–N–C–N(HisM200)–HOH–0 = (B_A) (see Brookhaven Protein Databank, 1PRC). A similar bridge is also seen on the B_B side of RCs (Fig. 4B) connecting P and B_B (H_B in *C. aurantiacus*). It is clear from the X-ray model presented in Fig. 4B that the maximal efficiency of ET from P* to B_A can occur when the wavepacket is on the $|+>$ surface having a maximal electron density on the P_B vacant orbital and optimal nuclear configuration for ET (the 935-nm emission from P*). The maximal efficiency of ET in *C. aurantiacus* from P* to H_B (which is located at the position of B_B in *Rp. viridis* RCs) can occur when the wavepacket is on the opposite side of the $|+>$ surface having maximal electron density on the P_A vacant orbital and optimal nuclear configuration for ET (the 895-nm emission from P*).

The estimation of the wavepacket energy gives a value of about 150 cm^{-1} (11 173 cm^{-1} (895 nm)-11 025 cm^{-1} (907 nm as 0–0 transition)) above the bottom of the P* surface. The intercrossing point is above the bottom by $\sim$30 cm^{-1} [14]. Therefore at the first, at 120 fs, and second, at 380 fs, approaches of the wavepacket to the intercrossing region the wavepacket energy should be above the intercrossing point by $\sim$120 cm^{-1}. According to [23] in this region the reflections from the walls of both wells (for the P* and $P^+B_A^-$ surfaces) are possible. The wavepacket at the P* surface wall emits light at 935 nm and at the $P^+B_A^-$ surface wall absorbs light at 1020 nm. In contrast to that the wavepacket on the opposite side of the P* surface emitting light at 895 nm and having the $P_A{*}P_B$ character induces ET from P* to H_B. It was found that the relative amplitudes of the oscillations at 120 fs delay for the 935- and 1020-nm bands are very similar in pheophytin-modified RCs (see also [14,25]) as estimated with respect to maximal amplitudes of corresponding ΔA found at 7 ps (0.19:0.20). This fact might suggest that each wavepacket approaching the long-wavelength side of the stimulated emission at 935 nm approaches the $P^+B_A^-$ surface as well. This is certainly not the case for ET from P* to H_B in *C. aurantiacus*, where the amplitude of the fs oscillations at 748 nm is much smaller ($\sim$0.03).

Acknowledgements: We thank Dr. A.V. Sharkov for help in maintenance of fs spectrometer, A.Ya. Shkuropatov and V.A. Shkuropatova for preparing the samples. This work was supported by Russian Basic Research Foundation (grant N 02-04-48650), NWO (The Netherlands) and INTAS grants.

References

[1] Deisenhofer, J., Epp, O., Miki, K., Huber, R. and Michel, H. (1984) Mol. Biol. 180, 385–398.
[2] Deisenhofer, J., Epp, O., Miki, K., Huber, R. and Michel, H. (1985) Nature 318, 618–624.
[3] Michel, H., Epp, O. and Deisenhofer, J. (1986) EMBO J. 5, 2445–2451.
[4] Komiya, H., Yeates, T.O., Rees, D.C., Allen, J.P. and Feher, G. (1988) Proc. Natl. Acad. Sci. USA 85, 9012–9016.
[5] Shuvalov, V.A., Klevanik, A.V., Sharkov, A.V., Matveetz, Yu.A. and Krukov, P.G. (1978) FEBS Lett. 91, 135–139.
[6] Shuvalov, V.A. and Duysens, L.N.M. (1986) Proc. Natl. Acad. Sci. USA 83, 1690–1694.
[7] Arlt, T., Schmidt, S., Kaiser, W., Lanterwasser, C., Meyer, M., Scheer, H. and Zinth, W. (1993) Proc. Natl. Acad. Sci. USA 90, 11757–11761.
[8] Chekalin, S.V., Matveetz, Yu.A., Shkuropatov, A.Ya., Shuvalov, V.A. and Yartzev, A.P. (1987) FEBS Lett. 216, 245–248.
[9] Schmidt, S., Arlt, T., Hamm, P., Huber, H., Nagele, T., Wachtveitl, J., Meyer, M., Scheer, H. and Zinth, W. (1994) Chem. Phys. Lett. 223, 116–120.
[10] Schmidt, S., Arlt, T., Hamm, P., Huber, H., Nagele, T., Wachtveitl, J., Zinth, W., Meyer, M. and Scheer, H. (1995) Spectrochim. Acta Part A 51, 1565–1578.
[11] Shkuropatov, A.Ya. and Shuvalov, V.A. (1993) FEBS Lett. 322, 168–172.
[12] Kennis, J.T.M., Shkuropatov, A.Ya., van Stokkum, I.H.M., Gast, P., Hoff, A.J., Shuvalov, V.A. and Aartsma, T.J. (1997) Biochemistry 36, 16231–16238.
[13] Yakovlev, A.G., Shkuropatov, A.Ya. and Shuvalov, V.A. (2000) FEBS Lett. 466, 209–212.
[14] Yakovlev, A.G. and Shuvalov, V.A. (2000) J. Chin. Chem. Soc. 47, 1–6.
[15] Franken, E.M., Shkuropatov, A.Ya., Franke, C., Neerken, S., Gast, P., Shuvalov, V.A., Hoff, A.J. and Aartsma, T.J. (1997) Biochim. Biophys. Acta 1321, 1–9.
[16] Shuvalov, V.A. and Yakovlev, A.G. (1998) Membr. Cell Biol. 12, 563–569.
[17] Vos, M., Rappaport, F., Lambry, J.-C., Breton, J. and Martin, J.-L. (1993) Nature 363, 320–325.
[18] Vos, M., Jones, M.R., Hunter, C.N., Breton, J., Lambry, J.-C. and Martin, J.-L. (1994) Biochemistry 33, 6750–6757.
[19] Streltsov, A.M., Vulto, S.I.E., Shkuropatov, A.Ya., Hoff, A.J., Aartsma, T.J. and Shuvalov, V.A. (1998) J. Phys. Chem. B 102, 7293–7298.
[20] Shuvalov, V.A., Klevanik, A.V., Ganago, A.O., Shkuropatov, A.Ya. and Gubanov, V.S. (1988) FEBS Lett. 237, 57–60.
[21] Cherepy, N.J., Shreve, A.P., Moore, L.J., Franzen, S., Boxer, S.G. and Mathies, R.A. (1994) J. Phys. Chem. 98, 6023–6029.
[22] Sokolov, A.A., Loskutov, Yu.M. and Ternov, I.M. (1962) Quantum Mechanics, Uchpedgiz, Moscow (in Russian).
[23] Ando, K. and Sumi, H. Nonequilibrium oscillatory electron transfer in bacterial photosynthesis, (1998) J. Phys. Chem. B 102, 10991–11000.

[24] Yakovlev, A.G., Shkuropatov, A.Ya. and Shuvalov, V.A. (2001) In: Abstracts of the XII Conference on Ultrafast Processes in Spectroscopy, UPS, Florence, Italy, p. 13.
[25] Yakovlev, A.G., Shkuropatov, A.Ya. and Shuvalov, V.A. (2002) Biochemistry 41, 2667–2674.
[26] Yakovlev, A.G., Shkuropatov, A.Ya. and Shuvalov, V.A. (2002) Biochemistry 41, 14019–14027.
[27] Streltsov, A.M., Aartsma, T.J., Hoff, A.J. and Shuvalov, V.A. (1997) Chem. Phys. Lett. 266, 347–352.
[28] Klevanik, A.V., Ganago, A.O., Shkuropatov, A.Ya. and Shuvalov, V.A. (1988) FEBS Lett. 237, 61–64.
[29] Johnson, S.G., Tang, D., Jankowiak, R., Hayes, J.M., Small, G.J. and Tiede, D.M. (1990) J. Phys. Chem. 94, 5849–5855.
[30] Parson, W.W., Chu, Z.T. and Warshel, A. (1998) Biophys. J. 74, 182–191.
[31] Parson, W.W., Chu, Z.T. and Warshel, A. (1998) Photosynth. Res. 55, 147–152.
[32] Sporlein, S., Zinth, W. and Watchtveitl, J. (1998) J. Phys. Chem. B 102, 7492–7496.
[33] Vos, H.M., Rischel, C., Jones, M.R. and Martin, J.-L. (2000) Biochemistry 39, 8353–8361.
[34] Shreve, A.P., Cherepy, N.J., Franzen, S., Boxer, S.G. and Mathies, R.A. (1991) Proc. Natl. Acad. Sci. USA 88, 11207–11211.
[35] Palaniappan, V., Aldema, M.A., Frank, H.A. and Bocian, D.F. (1992) Biochemistry 31, 11050–11058.
[36] Herzberg, H. (1949) Vibrational and Rotational Spectra of Multiatoms Molecules, Foreign Literature Publisher, Moscow.
[37] Gardner, K.H. and Kay, L.E. (1998) Annu. Rev. Biophys. Biomol. Struct. 27, 357–406.
[38] Michel, H. and Deisenhofer, J. (1988) Biochemistry 27, 1–7.
[39] Michel, H. and Deisenhofer, J. (1986) in: Photosynthesis III (Straehelin, L.A. and Arntzen C.J., Eds.), pp. 371–381, Springer, Berlin.
[40] Plato, M., Lendzian, F., Lubitz, W., Trankle, E. and Mobius, K. (1988) in: The Photosynthetic Bacterial Reaction Center: Structure and Dynamics (Breton, J. and Vermeglio, A., Eds.), pp. 379–388, Plenum Press, NY.
[41] Hamm, P., Gray, K.A., Oesterhelt, D., Feick, R., Scheer, H. and Zinth, W. (1993) Biochim. Biophys. Acta 1142, 99–105.
[42] Vos, M.H., Jones, M.R., Breton, J., Lambry, J.-C. and Martin, J.-L. (1996) Biochemistry 35, 2687–2692.
[43] Nagarajan, V., Parson, W.W., Davis, D. and Schenck, C. (1993) Biochemistry 32, 12324–12336.
[44] Jia, Y., DiMagno, T.J., Chan, C.-K., Wang, Z., Du, M., Hanson, D.K., Schiffer, M., Norris, J.R., Fleming, G.R. and Popov, M.S. (1993) J. Phys. Chem. 97, 13180–13191.
[45] Shochat, S., Arlt, T., Francke, C., Gast, P., Van Noort, P.I., Otte, S.C.M., Schelvis, H.P.M., Schmidt, S., Vijgenboom, E., Vrieze, J., Zinth, W. and Hoff, A.J. (1994) Photosynth. Res. 40, 55–66.
[46] Beekman, L.M.P., Van Stokkum, I.H.M., Monshouwer, R., Rijnders, A.J., McGlynn, P., Visschers, R.W., Jones, M.R. and Van Grondelle, R. (1996) J. Phys. Chem. 100, 7256–7268.
[47] McAuley, K.E., Fyfe, P.K., Cogdell, R.J., Isaacs, N.W. and Jones, M.R. (2000) FEBS Lett. 467, 285–290.
[48] Bixon, M., Jortner, J., Plato, M. and Michel-Beyerle, M.E. (1988) in: The Photosynthetic Bacterial Reaction center: Structure and Dynamics (Breton, J. and Vermeglio, A., Eds.), Plenum Press: NY, London, pp. 399–419.
[49] Nowak, F.R., Kennis, J.T.M., Franken, E.M., Shkuropatov, A.Ya., Yakovlev, A.G., Gast, P., Hoff, A.J., Aartsma, T.J. and Shuvalov, V.A. (1988) Proc. of the XI Int. Congr. on Photosynthesis, pp. 783–786, Budapest, Hungary, Kluwer, Academic Publishers, Dordrecht.
[50] Fleming, G.R., Martin, J.-L. and Breton, J. (1988) Nature 333, 190–192.
[51] Shuvalov, V.A., Shkuropatov, A.Y., Kulakova, S.M., Ismailov, M.A. and Shkuropatova, V.A. (1986) Biochim. Biophys. Acta 849, 337–348.
[52] Bruce, B.D., Fuller, R.C. and Blankenship, R.E. (1982) Proc. Natl. Acad. Sci. USA 79, 6532–6536.
[53] Shuvalov, V.A., Vasmel, H., Amesz, J. and Duysens, L.N.M. (1986) Biochim. Biophys. Acta 851, 361–368.
[54] Feick, R., Martin, J.-L., Breton, J., Volk, M., Landenbacher, T., Urbano, C., Ogrodnik, A. and Michel-Beyerle, M.E. (1990) in: Reaction Centers of Photosynthetic Bacteria (Michel-Beyerle, M.E., Eds.), pp. 181–188, Springer, Berlin.
[55] Becker, M., Nagarajan, V., Middendorf, D., Parson, W.W., Martin, J.E. and Blankenship, R.E. (1991) Biochim. Biophys. Acta 1057, 299–312.
[56] Hastings, G., Lin, S., Zhou, W. and Blankenship, R.E. (1993) Photochem. Photobiol. 57, 1–65.
[57] Feick, R., Shiozawa, J.A. and Ertlmaier, A. (1995) in: Anoxygenic Photosynthetic Bacteria (Blankenship, R.E., Madigan, M.T. and Bauer, C.E. Eds.), pp. 699–708, Kluwer Academic Publishers, Dordrecht.
[58] Shuvalov, V.A. (1990) Primary Light Energy Conversion at Photosynthesis, Nauka, Moscow (in Russian).
[59] Zhang, L.Y. and Friesner, R.A. (1998) Proc. Natl. Acad. Sci. USA 95, 13603–13605.